Dynamics Study of the $O_2 + HO_2$ Atmospheric Reaction with Both Reactants Highly Vibrationally Excited

L. Zhang and A. J. C. Varandas*

Departamento de Química, Universidade de Coimbra, P-3049 Coimbra Codex, Portugal

Received: July 11, 2002; In Final Form: September 30, 2002

We report a theoretical study of the title five-atom atmospheric reaction for vibrationally excited states of O_2 over the range $18 \leq v \leq 27$, and initial vibrational energies of HO_2 over the range $36 \leq E_v/\text{kcalmol}^{-1} \leq 51$. All calculations have employed the quasiclassical trajectory method and the realistic double many-body expansion potential energy surface recently reported for $HO_4(^2A)$. The results indicate that it can be a potential source of ozone in the upper atmosphere.

1. Introduction

Vibrationally excited molecules play a central role in several areas of chemical dynamics and kinetics. Knowledge of the collisional process of such molecules is therefore vital to gain insight into their chemical and physical properties. In fact, the influence of vibrational excitation on the rates of bimolecular reactions has been of longstanding interest in chemical reaction dynamics. As such, uncovering the dynamics of these reactive processes can greatly enhance our understanding of atmospheric chemistry, combustion, and unimolecular decomposition of activated species.[1−5] Of particular importance is the role of internal energy in the collisional process, especially for energies near the dissociation threshold. The energy dependence holds important information about the behavior of molecules at high energies and can provide clues as to the microscopic details of intermolecular energy transfer.[6]

Vibrationally excited molecular oxygen [hereafter denoted by $O_2(v)$], generated in the ultraviolet photolysis of ozone, has recently been proposed[7−10] to explain the limitations of traditional atmospheric ozone models.[11−13] In fact, models of atmospheric chemistry have consistently underpredicted the measured ozone concentrations in the upper stratosphere and mesosphere in recent years. Such an "ozone deficit" problem is even more troubling because it occurs in a part of the atmosphere which is considered to be well understood. As a result, recent attempts to overcome this problem have focused on identifying new sources of ozone,[7,14−21] since the known ozone loss mechanisms appear to be accurately understood and any that have been overlooked can only increase the existing discrepancy.

Because of its atmospheric importance, the collisional processes of $O_2(v)$ have become among the most extensively studied sets of examples of collisional dynamics involving highly vibrationally excited molecules. In fact, the past decade or so has seen considerable effort, both experimental and theoretical, aimed at yielding a complete picture for $O_2(v)$ in collisions with a variety of atmospheric constituents such as O_2, O_3, OH, N_2, CO_2, NO_2, and N_2O. Although significant progress has been made in measuring the vibrational level dependence of the total removal rate constants in these collisional processes,[7,8,14,15,17−25] an important natural species of the atmosphere which is remarkably absent from such a progress list is HO_2. In fact, the HO_2 radical is a key intermediate for many chemical reactions in atmospheric chemistry.[26−33] Recently, a novel catalytic source of ozone[34,35] has been proposed, which suggests that the $O_2(v) + HO_2$ (E_v) reaction may have important implications in modeling the upper stratospheric and mesospheric ozone concentration. An investigation of the collisional properties of highly vibrationally excited O_2 with HO_2 radicals is therefore an intriguing topic of considerable interest, which we will examine in the present work.

In a previous paper (hereafter referred to as paper I[36]), we have provided the first information on collisions of vibrationally excited molecular oxygen with the hydroperoxyl radical in its ground vibrational state ($E_0 = 8.490$ kcal mol^{-1}). However, our understanding of the collisional processes of these species is far from complete since the role of reactants internal energy in such processes has partically been left unanswered. A need therefore exists to identify important physical parameters and propensities in such collisional processes. In addition to its relevance in atmospheric chemistry, the $O_2(v) + HO_2(E_v)$ atmospheric reaction can per se be interesting as a prototype of a diatomic−triatomic bimolecular collision process involving both reactant molecules in vibrationally excited states.

A major aim of the present work is therefore to report a detailed theoretical study of the title multichannel reaction

$$O_2(v) + HO_2(E_v) \rightarrow O_3^*/O_3 + OH \quad (1)$$

$$\rightarrow O_2 + O_2 + H \quad (2)$$

$$\rightarrow O_2 + OH + O \quad (3)$$

$$\rightarrow HO_2 + O + O \quad (4)$$

by considering the vibrationally excited states of O_2 over the range $18 \leq v \leq 27$ and the HO_2 molecules containing between 36 and 51 kcal mol^{-1} of vibrational excitation. Such combinations will be heretofore denoted by (v, E_v), with E_v assumed to be given in kcal mol^{-1}. Note that the star in reaction 1 indicates that the formed ozone molecules have an internal energy above the dissociation limit. Thus, they will ultimately decompose through the unimolecular dissociation reaction

* To whom correspondence should be addressed. E-mail: varandas@qtvsl.qui.uc.pt.

10.1021/jp021595i CCC: $22.00
Published on Web 11/12/2002

$$O_3^* \rightarrow O_2 + O \quad (5)$$

or will stabilize in the presence of some inert species M via the inelastic process

$$O_3^* + M \rightarrow O_3 + M \quad (6)$$

Other interesting channels in relation to ozone formation are reactions 3 and 4, which involve reactants dissociation under such conditions. Indeed, dissociation of both reactants lead to formation of atomic oxygen, which will then form ozone by the three-body recombination reaction

$$O(^3P) + O_2 + M \rightarrow O_3 + M \quad (7)$$

For the dynamics calculations, we will employ the quasi-classical trajectory (QCT) method and the realistic single-valued DMBE (double many-body expansion[37,38]) potential energy surface[39] for the electronic ground state of HO_4, which has been extensively used to study the $OH(v) + O_3$ atmospheric reaction.[39−41] Good agreement was obtained in this case with the available experimental data. Note that an accurate quantum dynamics study of the title reaction is currently out of reach mostly due to computational limitations (ref 18, and references therein).

The paper is organized as follows. Section 2 provides a brief survey of the $HO_4(^2A)$ DMBE potential energy surface, while the computational method is described in section 3. The dynamics results are presented and disscussed in section 4, while the major conclusions are in section 5.

2. Potential Energy Surface

As in paper I, all calculations reported in this work have employed a full-dimensional (9D) DMBE potential energy surface[39] for the ground electronic state of HO_4. Since it has been described in detail elsewhere,[36,39−41] we report in Figure 1 only the minimum energy path for reaction 1 and some energetic features which are of relevance for the present work. These refer to the energetics for various combinations of vibrational excitation and relevant product channels according to the HO_4 DMBE potential energy surface. As is seen, the internal energy combinations on the reactants side not only are quite above the energy of the transition state for reaction 1, but are higher than the energy of the product channels leading to $O_2 + O_2 + H$ and $O_2 + OH + O$ formation. This implies that the reactions 1−3 are feasible over the complete range of translational energies. Note that, for the internal energy combination (20, 51), the reactive channel leading to $HO_2 + O + O$ is just barely open. However, for combinations involving higher internal energies, all reactive channels ($O_3^*/O_3 + OH$, $O_2 + O_2 + H$, $O_2 + OH + O$, and $HO_2 + O + O$) are accessible over the complete range of translational energies.

3. Computational Details

Following paper I, the QCT method has been employed as implemented in an extensively adapted version of the MERCURY/VENUS96[42] code. As summarized in Table 1, calculations have been carried out for diatom−triatom translational energies over the range $1.0 \leq E_{tr}/\text{kcal mol}^{-1} \leq 20.0$. Except for some check cases, the initial rotational quantum number of the colliding $O_2(v)$ has been fixed at the ground level ($j = 1$). In fact, since the O_2 molecules are highly vibrationally excited, one expects to a first approximation the initial rotational excitation to play a minor role. In fact, a quantitative assessment of this assumption will also be reported. Meanwhile, the total vibrational energy of HO_2, $E_v = \sum_{k=1}^{3} E_{v_k}$, where E_{v_k} indicates the energy content of the various vibrational normal modes of the triatomic molecule. Note that the chosen vibrational-excitation energy range for $HO_2(E_v)$ mimics roughly that observed for the products of the $OH(v \leq 4) + O_3$ reaction.[41] Note, especially, that it covers internal energies of the triatomic up to near dissociation. Furthermore, in the absence of any a prior information on the energy distribution among the various normal modes, we have assumed a democratic distribution for it. Such a choice may find support on previous classical trajectory studies of the $HO_2 \rightarrow H + O_2$ unimolecular process for energies just above dissociation, which have shown to display RRKM-type (i.e., a single-exponential-type) behavior for nonrotating HO_2, with a double-exponential curve being necessary to fit the trajectory data when rotational excitation is added to the system.[43,44] In turn, the rotational energy about each principal axis of inertia of HO_2 has been taken as $k_BT/2$, while the rotational temperature has been assumed to be 300 K. This corresponds to an intermediate value over the range of temperatures $100 \leq T/\text{K} \leq 500$, which are likely to be the ones of major interest for atmospheric chemistry. Working parameters for numerical integration and maximum value of the impact parameter (b_{max}) have been determined as in paper I. Similarly, the initial diatom−triatom separation has been fixed at 17 a_0 to make the interaction essentially negligible. Batches of 2000 trajectories have been carried out for each translational energy and vibrational combination making a total of 9.2×10^4 trajectories. Such a number of trajectories is enough to yield reactive cross sections with an error smaller than about (10%) for all translational energies considered in the current work.

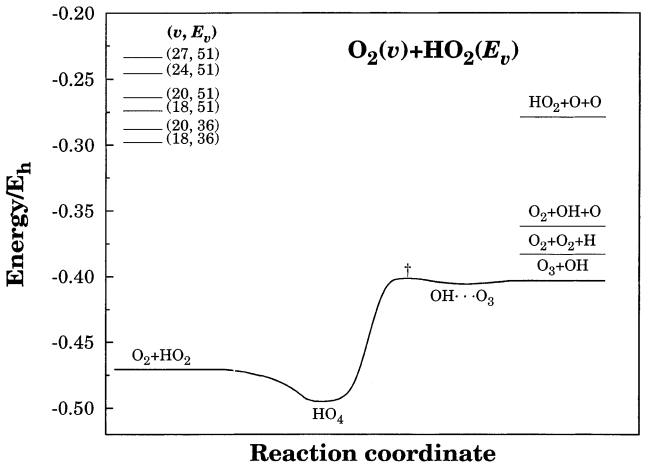

Figure 1. Minimum energy path for formation of $O_3^*/O_3 + OH$. The saddle point geometry is indicated by the symbol †. Also shown are the relevant energetics of the title reaction according to the HO_4 DMBE potential energy surface.

For a specified translational energy, all relevant reactive cross sections and associated 68% uncertainties have been calculated. They will be denoted σ^x and $\Delta\sigma^x$, respectively, with x specifying the reaction outcome; $x = total$ stands for formation of $O_3^*/O_3 + OH$, $O_2 + O_2 + H$, $O_2 + OH + O$, and $HO_2 + O + O$. From the cross sections, and assuming a Maxwell−Boltzmann distribution over the translational energy, the specific thermal rate coefficients are obtained as

$$k^x(T) = g_e(T)\left(\frac{2}{k_BT}\right)^{3/2}\left(\frac{1}{\pi\mu}\right)^{1/2}\int_0^\infty E_{tr}\sigma^x \exp\left(-\frac{E_{tr}}{k_BT}\right) dE_{tr} \quad (8)$$

TABLE 1: Summary of the $O_2(v) + HO_2(E_v)$ Trajectory Calculations

(v, E_v)	E_{tr} (kcal mol^{-1})	b_{max} (a_0)	$O_3^*/O_3 + OH$ N_r	$O_2 + O_2 + H$ N_r	$O_2 + OH + O$ N_r	$HO_2 + O + O$ N_r	$\sigma^{total} \pm \Delta\sigma^{total}$ (a_0^2)
(27, 36)	1.0	12.09	92	168	425	2	157.85 ± 4.88
	2.0	10.96	111	180	372	2	125.49 ± 3.98
	4.0	9.45	98	169	435	8	99.57 ± 3.00
	6.0	9.07	97	158	443	4	90.73 ± 2.76
	8.0	8.88	103	140	423	3	82.90 ± 2.61
	12.0	8.50	88	125	402	8	70.77 ± 2.35
	16.0	8.31	71	111	424	10	66.90 ± 2.24
(27, 42)	1.0	12.09	110	322	456	5	205.18 ± 5.11
	2.0	10.96	100	281	425	5	153.04 ± 4.14
	4.0	9.64	98	280	447	11	121.97 ± 3.22
	6.0	9.26	88	254	434	6	105.32 ± 2.94
	8.0	8.88	104	216	440	13	95.78 ± 2.70
	12.0	8.88	72	206	383	5	82.53 ± 2.61
	16.0	8.50	81	181	402	11	76.67 ± 2.40
(27, 48)	1.0	12.28	100	439	428	19	233.68 ± 5.30
	2.0	10.96	103	437	401	6	178.70 ± 4.21
	4.0	10.39	81	367	388	9	143.38 ± 3.75
	6.0	9.64	77	385	393	12	126.50 ± 3.23
	8.0	9.26	86	334	440	14	117.71 ± 2.99
	12.0	9.07	56	293	427	17	102.49 ± 2.83
	16.0	8.88	72	278	410	15	96.03 ± 2.70
(27, 51)	1.0	12.28	106	518	456	13	259.04 ± 5.28
	2.0	11.15	88	500	408	14	197.22 ± 4.37
	4.0	10.20	105	461	377	15	156.70 ± 3.65
	6.0	9.64	79	442	417	15	138.61 ± 3.26
	8.0	9.83	76	368	391	8	127.87 ± 3.35
	12.0	9.07	78	359	424	18	113.60 ± 2.87
	16.0	8.88	57	323	433	22	103.47 ± 2.73
(18,36)	1.0	10.77	33	47	110		34.63 ± 2.39
	2.0	9.83	36	46	102		27.91 ± 1.96
	4.0	8.88	38	45	90		21.44 ± 1.56
	6.0	8.31	35	39	111		20.09 + 1.41
	8.0	8.13	34	32	102		17.42 ± 1.29
	12.0	7.94	28	41	91		15.83 ± 1.20
(20, 36)	1.0	11.53	50	67	163		58.44 ± 3.24
	2.0	9.64	50	81	172		44.21 ± 2.34
	4.0	9.07	47	61	157		34.25 ± 1.96
	6.0	8.69	33	55	180		31.81 ± 1.81
	8.0	8.50	37	46	161		27.72 ± 1.66
	12.0	8.13	40	50	150		24.89 ± 1.51
(24, 36)	1.0	11.72	96	153	309		120.32 ± 4.33
	2.0	10.39	84	133	318		90.78 ± 3.36
	4.0	9.26	88	137	317		73.00 ± 2.68
	6.0	8.88	65	118	346		65.55 ± 2.44
	8.0	8.69	82	103	322		60.18 ± 2.31
	12.0	8.13	66	108	326	1	51.96 ± 2.01

where $g_e(T) = {}^1/_3$ is the electronic degeneracy factor which corresponds to the ratio of the electronic partition functions, k_B is the Boltzmann constant, μ is the reduced mass of the colliding particles, and T is the temperature.

4. Results and Discussion

Table 1 provides a summary of the trajectory calculations reported in the present work. Column one indicates the vibrational combination while the studied translational energies are in column two. For these initial translational energies, the dominant open reactive channels leading to products are

$$O_aO_b + HO_dO_c \rightarrow O_aO_bO_c + O_dH \quad (9)$$

$$\rightarrow O_aO_b + O_cO_d + H \quad (10)$$

$$\rightarrow O_aO_b + O_dH + O_c \quad (11)$$

$$\rightarrow O_aO_c + O_dH + O_b \quad (12)$$

$$\rightarrow O_bO_c + O_dH + O_a \quad (13)$$

$$\rightarrow HO_dO_c + O_a + O_b \quad (14)$$

where the indices *a*, *b*, *c*, and *d* label the four different oxygen atoms. As in paper I, reaction 9 indicates formation of $O_3^*/O_3 + OH$ products via an oxygen atom abstraction mechanism. Note that the reactions in eqs 12 and 13 have identical probabilities of occurrence, with the reaction in eq 11 having a small percentage of occurrence compared with such reactive channels. Note further that a detailed analysis of these reactive channels has been done in paper I. The difference now is that, for vibrationally excited HO_2, the probability of breaking its bonds increases, and hence the fractions of such products shows a significant growth. However, the reaction in eq 14 shows a low probability of occurrence, with the corresponding reactive cross section being an order of magnitude smaller than those of the process yielding other products. This by no means implies that the formation of $HO_2 + O + O$ provides a negligible contribution to the dynamics and kinetics of the title reaction. Indeed, such a process contributes twice as a source of ozone, since each atom ultimately leads to an O_3 molecule through the three-body recombination reaction with molecular oxygen. In summary, processes leading to formation of $O_3^*/O_3 + OH$, $O_2 + O_2 + H$, and $O_2 + OH + O$ hold a dominant position for

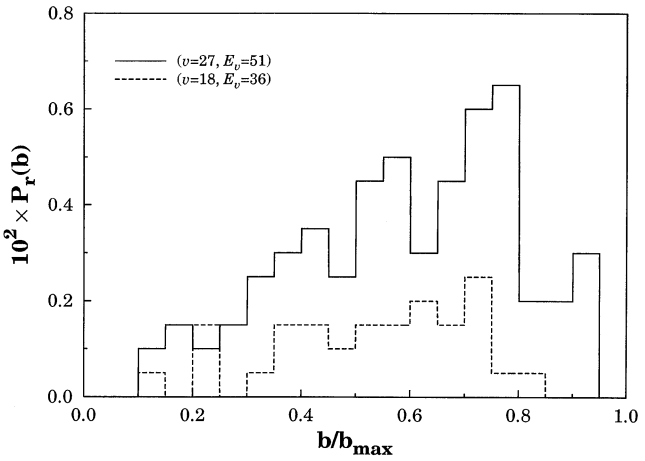

Figure 2. Opacity function for formation of O_3^*/O_3.

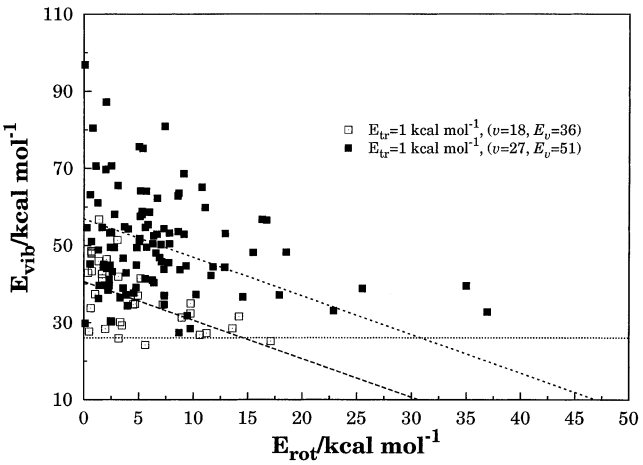

Figure 3. Vibrational-rotational energy distribution of products O_3^*/O_3. The dotted line indicates the threshold energy for dissociation into $O_2 + O$, while the dashed line shows lines constant $E_{vib} + E_{rot}$ values.

the title reaction. For the higher vibrational energy combinations, formation of $O_2 + O_2 + H$ and $O_2 + OH + O$ may play a more prominent role than $O_3^*/O_3 + OH$.

The dependence of the maximum impact parameter on translational energy for the title reaction is shown in Table 1. As expected, the maximum impact parameter increases with internal energy of the reactants for a fixed translational energy. Conversely, b_{max} is found to increase with decreasing translational energy, as it usually happens for reactions that occur via a capture-type mechanism. These observations may be rationalized from the fact that dominant interactions between O_2 and HO_2 are, at large distances, of the dipole−dipole and dipole−quadrupole electrostatic types. In fact, since the reactants are vibrationally excited (such a stretching leads to an increase of both the dipole and quadrupole moments over the range of the excitations considered in present work), one expects the attractive long-range forces to increase for the most favorable approaching orientations.

Figure 2 shows a typical opacity function for formation of $O_3^*/O_3 + OH$. Note that the abcissae in these plots are b/b_{max}, with b_{max} being the largest impact parameter found in the present work (12.28 a_0). The notable feature from this figure is the fact that the opacity function shows a single pattern: it increasees with impact parameter, which is an indication that long-range forces may be playing an important role.

Using the model developed in ref 41 we have estimated the average lifetime of the formed O_3^*/O_3 species for typical capture-type [($v = 20$, $E_v = 51$), ($v = 27$, $E_v = 51$), $E_{tr} = 1.0$ kcal mol^{-1}] processes to be 0.321 and 0.305 ps, respectively. We recall that in paper I we have obtained for O_2 ($v = 20$, 27) at the same translational energy the corresponding values of 0.627 and 0.442 ps (the reactant hydroperoxyl radical was in its ground vibrational state). As one might expect, for a fixed translational energy and vibrational state of O_2, such a lifetime is seen to decrease with increasing internal energy of the HO_2 molecule. This result may be explained by recalling that the majority of the O_3^*/O_3 species are produced through a rapid flux of energy to the O−O stretch mode, which is a more likely event when HO_2 is vibrationally excited.

Figure 3 displays the vibrational−rotational distribution of product O_3^*/O_3 for two distinct vibrational combinations [($v = 18$, $E_v = 36$) and ($v = 27$, $E_v = 51$)] at $E_{tr} = 1.0$ kcal mol^{-1}. The dotted line indicates the threshold energy for dissociation of O_3^* into $O_2 + O$, while in dash are the lines corresponding to constant averaged internal energies ($E_{vib} + E_{rot}$). Clearly, almost all formed ozone molecules have a substantial amount of internal energy which is above the dissociation limit. Thus, such vibrationally hot ozone (O_3^*) molecules will finally lead to formation of stable ozone species via either a quenching mechanism or through dissociation followed by fast recombination of the formed oxygen atom in excess of molecular oxygen.

We now examine the shapes of the excitation functions (cross section vs translational energy) for formation of all products, which are shown in Figure 4 together with the associated 68% error bars (a separate examination of the cross section leading to $HO_2 + O + O$ has been reported elsewhere in the context of a theoretical reappraisal of the HO_x atmospheric cycle[35]). Two distinct combinations of internal energies are considered. In both cases, the vibrational energy of one of the reactant species is fixed at a specific state while its reactive partner contains a flexible vibrational excitation covering the whole range of energies considered in the present work. Such a procedure may provide us with important insights into the role of the reactants internal energy, thus highlighting the general trends of the title reaction. It is clear that the reactive cross sections show a markedly decreasing pattern with translational energy. Such a fact suggests that a capture-type mechanism dominates over the studied range of translational energies. We recall from paper I that, although reactive $O_2(v)$ removal via a capture-type mechanism plays a leading role over the whole range of translational energies, both capture- and barrier-type mechanisms have been encountered for low and high translational energies. Such different behaviors can only be attributed to the high internal energies arising from the vibrational energy of the HO_2 molecules. In fact, the HO_2 vibrational energy effectively promotes rupture of its bonds while enhancing the role of long-range forces in the formation of products.

To analytically describe the dependence of the cross section with the translational energy, we have adopted the form

$$\sigma^x(E_{O_2}, E_{HO_2}, E_{tr}) = \frac{\sum_{k=1}^{3} c_k E_{sum}^k}{E_{tr}^{n_1}} \qquad (15)$$

where $E_{sum} = E_{O_2} + E_{HO_2}$, with E_{O_2} and E_{HO_2} being the internal energies of the O_2 and HO_2 molecules. Note that such a representation depends only on the internal energy of the reactant species but not on any specific model which expresses the dependence of the internal energy with the quantum

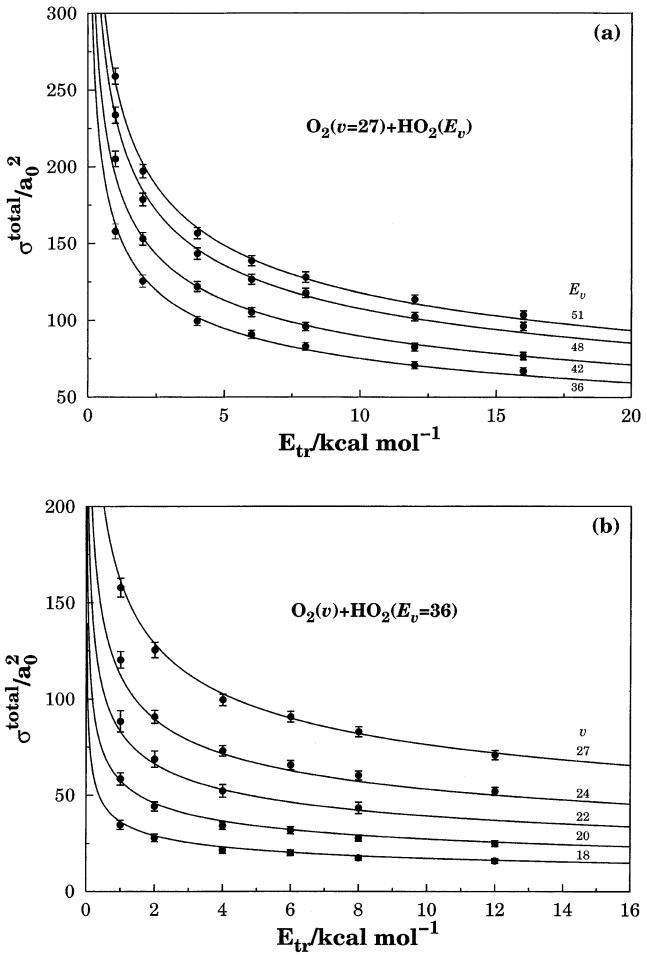

Figure 4. Reactive total cross section σ^{total} for formation of $O_3^*/O_3 + OH$, $O_2 + O_2 + H$, $O_2 + OH + O$, and $HO_2 + O + O$. Also indicated are the 68% error bars and the fitted line given by eq 15: (a) ($v = 27$, E_v) and (b) (v, $E_v = 36$ kcal mol^{-1}).

TABLE 2: Numerical Values of Least-Squares Parameters in Equation 15[a]

parameter	($v = 27$, E_v)	(v, $E_v = 36$)
c_1	6.15995	2.69505
c_2	−9.98575(−2)[b]	−6.69957(−2)
c_3	4.68652(−4)	4.15331(−4)
n_1	0.335470	0.325019

[a] Units are such that with the energy in kcal mol^{-1}, the cross section is a_0^2. [b] Given in parentheses are the powers of 10 by which the numbers should be multiplied. For reproducibility, six significant figures are reported, although this by no means imply that the coefficients are known to such an accuracy.

numbers. All the parameters have been determined from a least-squares fitting procedure, with their optimum values being reported in Table 2. The resulting fitted functions are exhibited together with the calculated points in Figure 4. It is seen that the fitting forms show very good agreement with the calculated points and, hence, reflect the general trends of the calculations. It also suggests that it may be reliable in predicting the cross section in panel (b) for other v states not specifically considered in this work, as it can be seen from the data calculated for $v = 22$ (these employed only 10^3 trajectories per point) which has not been included in the least-squares fitting procedure. Of course, care must be exercised when using the above model excitation function to extrapolate far beyond the range of v and E_{tr} values considered in the fit [shown by the solid dots in Figure 4.

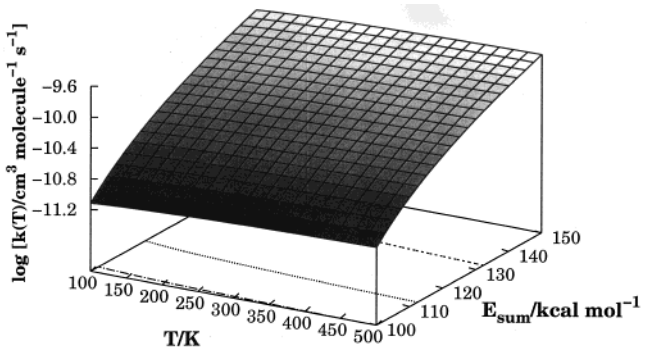

Figure 5. Total reactive thermal rate coefficient for $O_2(v) + HO_2$ ($E_v = 36$ kcal mol^{-1}) as a function of temperature and sum of the reactants internal energies. Lines in the contour plot are spaced by $10^{0.5}$ cm^3 molecule^{-1} s^{-1} starting at 10^{-12} cm^3 molecule^{-1} s^{-1}.

TABLE 3: Calculated Specific Rate Coefficients for Formation of All Products at 298 K

(v, E_v)	E_{sum} (kcal mol^{-1})	k_{v,E_v} (cm^3 molecule^{-1} s^{-1})	k_{v,E_0}[a] (cm^3 molecule^{-1} s^{-1})
(18, 36)	109.3	2.27(−11)	1.70(−13)
(20, 36)	115.5	3.59(−11)	2.93(−12)
(24, 36)	127.0	6.97(−11)	3.04(−11)
(27, 36)	134.5	1.00(−10)	5.83(−11)
(27, 42)	140.5	1.21(−10)	
(27, 48)	146.5	1.46(−10)	
(27, 51)	149.5	1.60(−10)	

[a] From ref 36: HO_2 is in its ground vibrational state ($E_o = 8.490$ kcalmol^{-1}).

By substitution of eq 15 in eq 8 and performing the integration analytically, one obtains for the specific thermal rate coefficients

$$k_E(T) = g_e(T)\left(\frac{8}{\pi\mu}\right)^{1/2}\left(\sum_{i=1}^{3} c_i E_{sum}^i\right)\Gamma(2-n_1)(RT)^{-n_1+1/2} \quad (16)$$

where $\Gamma(...)$ is the gamma function, and all other symbols have their usual meaning. Figure 5 shows as a perspective plot of the $O_2(v) + HO_2(E_v = 36)$ total reactive rate constant (i.e., for formation of products: $O_3^*/O_3 + OH$, $O_2 + O_2 + H$, $O_2 + OH + O$, and $HO_2 + O + O$) as a function of temperature and the sum of reactants internal energies. Note that similar considerations apply to the case of $O_2(v=27) + HO_2$ (E_v). Since their shapes differ only quantitatively, we show only the first case in Figure 5. The notable feature is perhaps the significant increase of the rate constant with increasing reactant internal energy and temperature.

Table 3 compares the calculated thermally averaged specific rate coefficients at 298 K. As shown, the rate constants are seen to vary only within a 5-fold factor when going from $v = 18$ to $v = 27$ for a fixed vibrational energy content of HO_2. However, for $v = 18$, the rate constant is found to be 2 orders of magnitude larger than the corresponding value in paper I when HO_2 is considered to be in its ground vibrational state. Such a remarkable discrepancy reflects the influence of the HO_2 reactant internal energy content. As it might be expected, such an influence is found to decrease with increasing internal energy of O_2. In fact, for highly vibrationally excited levels of O_2 such as $v = 27$, the rate constants reported in paper I can be over one-half of the values reported in the present work. Thus, the rate constants for the title multichannel reaction are strongly influenced by the reactants internal energy content.

Figure 6 shows cuts of Figure 5 for $v = 18$, 20, 24, and 27. Also shown by the dots in Figure 6 are the results obtained

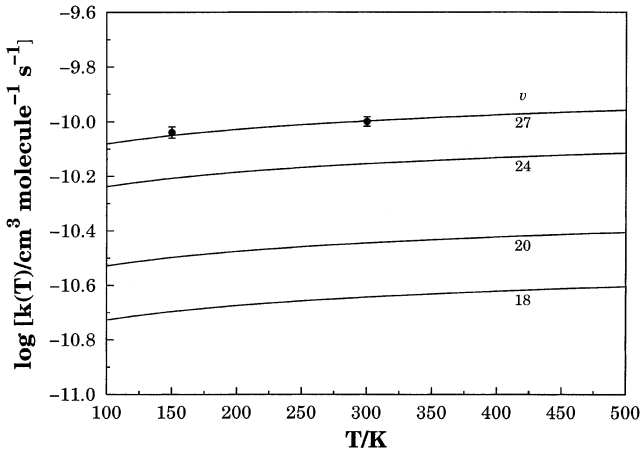

Figure 6. Cuts in Figure 5 for $v = 18$, 20, 24, and 27. The dots indicate the results of calculations using thermally averaged rotational distributions for O_2.

from rotationally averaged calculations for $v = 27$ and $E_v = 36$ kcal mol^{-1} using 2×10^3 trajectories. As expected, such results suggest that the trends reported in this work for O_2 kept at $j = 1$ should not differ drastically from those obtained for a thermalized rotational distribution.

5. Conclusions

Despite its potential atmospheric importance, the title multichannel reaction had not been studied thus far theoretically due to lack of a realistic potential energy surface. One of our major motivations in this work has therefore been to cover such a gap, and hence aim at yielding a complete series of studies by using our recently proposed DMBE potential energy surface for the ground doublet state of HO_4.[39] Specifically, we have carried out a QCT study of the title reaction for several combinations of vibrational excitations of the reactant species. The calculations have shown that the product ozone molecules are formed exclusively via an oxygen-atom abstraction following a capture-type mechanism in which long-range forces seem to play an important role both at low and high translational energies. With the increasing vibrational energy of the HO_2 molecules, such an abstraction reaction occurs via prompt breaking and formation of the O−O bonds, and hence, the lifetime of the ozone species is rather short. The calculations also suggest that the title multichannel reaction is well described by a capture-type excitation function over the whole range of translational energies. In contrast with paper I, the corresponding rate constants have been shown to vary drastically with the vibrational combination of reactant species. Although no comparison with experimental data is possible at present (to our knowledge, no experimental evidence of the title multichannel reaction has been reported), the results from the present work suggest that the title reactive processes can be a potential source of ozone in the upper atmosphere. Thus, they should be taken into consideration when identifying new ozone resources. In the same sense, experimental studies using laser techniques that allow for the preparation of vibrationally hot reactant molecules would be greatly welcome for the title system.

Acknowledgment. The support of Fundação para a Ciência e Tecnologia, Portugal, under program PRAXIS XXI is gratefully acknowledged.

References and Notes

(1) Mullin, A. S., Schatz, G. C., Eds. *Highly Excited Molecules: Relaxation, Reaction and Structure*; American Chemical Society Books: Washington, DC, 1997.

(2) Weston, R. E.; Flynn, G. W. *Annu. Rev. Phys. Chem.* **1992**, *43*, 559.

(3) Gilbert, R. G.; Smith, S. C. *Theory of Unimolecular and Recombination Reactions;* Blackwell Scientific Publications: Oxford, 1990.

(4) Oref, I.; Tardy, D. C. *Chem. Rev.* **1990**, *90*, 1407.

(5) Gordon, R. *Comments At. Mol. Phys.* **1988**, *21*, 123.

(6) Wall, M. C.; Lemoff, A. S.; Millin, A. S. *J. Phys. Chem. A* **1998**, *102*, 9101.

(7) Price, J. M.; Mack, J. A.; Rogaski, C. A.; Wodtke, A. M. *Chem. Phys.* **1993**, *175*, 83.

(8) Rogaski, C. A.; Price, J. M.; Mack, J. A.; Wodtke, A. M. *Geophys. Res. Lett.* **1993**, *20*, 2885.

(9) Miller, R. L.; Suits, A. G.; Houston, P. L.; Toumi, R.; Mack, J. A.; Wodtke, A. M. *Science* **1994**, *265*, 1831.

(10) Houston, P. L. *Acc. Chem. Res.* **1995**, *28*, 453.

(11) Eluszkiewicz, M. A. J.; Allen, M. *J. Geophys. Res.* **1993**, *98*, 1069.

(12) Siskind, D. E.; Connor, B. J.; Remsberg, R. S. E. E. E.; Tsou, J. J.; Parrish, A. *J. Geophys. Res.* **1995**, *100*, 11191.

(13) Osterman, G. B.; Salawitch, R. J.; Sen, B.; Toon, G. C.; Stachnik, R. A.; Pickett, H. M.; Margitan, J. J.; Blavier, J.; Peterson, D. B. *Geophys. Res. Lett.* **1997**, *24*, 1107.

(14) Varandas, A. J. C.; Wang, W. *Chem. Phys.* **1997**, *215*, 167.

(15) Wang, W.; Varandas, A. J. C. *Chem. Phys.* **1998**, *236*, 181.

(16) Varandas, A. J. C.; Pais, A. A. C. C.; Marques, J. M. C.; Wang, W. *Chem. Phys. Lett.* **1996**, *249*, 264.

(17) Garrido, J. D.; Caridade, P. J. S. B.; Varandas, A. J. C. *J. Phys. Chem.* **1999**, *103*, 4815.

(18) Varandas, A. J. C. *Int. Rev. Phys. Chem.* **2000**, *19*, 199.

(19) Varandas, A. J. C.; Caridade, P. J. S. B. *Chem. Phys. Lett.* **2001**, *339*, 1.

(20) Caridade, P. J. S. B.; Zhang, L.; Garrido, J. D.; Varandas, A. J. C. *J. Phys. Chem. A* **2001**, *105*, 4395.

(21) Caridade, P. J. S. B.; Betancourt, M.; Garrido, J. D.; Varandas, A. J. C. *J. Phys. Chem. A* **2001**, *105*, 7435.

(22) Parker, H.; Slanger, T. G. *J. Chem. Phys.* **1994**, *100*, 287.

(23) Mack, J. A.; Mikulecky, K.; Wodtke, A. M. *J. Chem. Phys.* **1996**, *105*, 4105.

(24) Balakrishnan, N.; Billing, G. D. *Chem. Phys. Lett.* **1995**, *242*, 68.

(25) Balakrishnan, N.; Dalgarno, A.; Billing, G. D. *Chem. Phys. Lett.* **1998**, *288*, 657.

(26) Bates, D. R.; Nicolet, M. *J. Geophys. Res.* **1950**, *55*, 301.

(27) Hunt, B. G. *J. Geophys. Res.* **1966**, *71*, 1385.

(28) Nicolet, M. *Planet. Space Sci.* **1972**, *20*, 1671.

(29) Rowland, F. S.; Molina, M. *Rev. Geophys. Space Phys.* **1975**, *13*, 1.

(30) Nicolet, M. *Rev. Geophys. Space Phys.* **1975**, *13*, 593.

(31) Kaufman, F. *Annu. Rev. Phys. Chem.* **1979**, *30*, 411.

(32) Chang, J. S.; Duewer, W. H. *Annu. Rev. Phys. Chem.* **1979**, *30*, 443.

(33) Nicolet, M. *Adv. Chem. Phys.* **1985**, *55*, 63.

(34) Varandas, A. J. C. *ChemPhysChem* **2002**, *3*, 433.

(35) Varandas, A. J. C. To be submitted for publication.

(36) Zhang, L.; Varandas, A. J. C. *J. Phys. Chem. A* **2001**, *105*, 10347.

(37) Varandas, A. J. C. *Adv. Chem. Phys.* **1988**, 74, 255.

(38) Varandas, A. J. C. *Lecture Notes in Chemistry;* Laganá, A., Riganelli, A., Eds.; Springer: Berlin, 2000; Vol. 75, p 33.

(39) Varandas, A. J. C.; Zhang, L. *Chem. Phys. Lett.* **2000**, *331*, 474.

(40) Varandas, A. J. C.; Zhang, L. *Chem. Phys. Lett.* **2001**, *340*, 62.

(41) Zhang, L.; Varandas, A. J. C. *Phys. Chem. Chem. Phys.* **2001**, *3*, 1439.

(42) Hase, W. L.; Duchovic, R. J.; Hu, X.; Komornicki, A.; Lim, K. F.; Lu, D.; Peslherbe, G. H.; Swamy, K. N.; Linde, S. R. V.; Varandas, A. J. C.; Wang, H.; Wolf, R. J. *QCPE Bull.* **1996**, *16*, 43.

(43) Marques, J. M. C.; Varandas, A. J. C. *J. Phys. Chem.* **1997**, *101*, 5168.

(44) Marques, J. M. C.; Llanio-Trujillo, J. L.; Varandas, A. J. C. *Phys. Chem. Chem. Phys.* **2000**, *2*, 3583.